Design and Testing of a Scaled Demonstrator Turbine at the National Wind Technology Center

Preprint

Christopher J. Bay,[1] Rick Damiani,[1] Lee Jay Fingersh,[1]
Scott Hughes,[1] Mayank Chetan,[2] Shulong Yao,[2] D. Todd Griffith,[2]
Gavin K. Ananda,[3] Michael S. Selig,[3] Daniel S. Zalkind,[4]
Lucy Y. Pao,[4] Dana Martin,[5] Kathryn E. Johnson,[5]
Meghan Kaminski,[6] and Eric Loth[6]

1 National Renewable Energy Laboratory
2 University of Texas
3 University of Illinois
4 University of Colorado
5 Colorado School of Mines
6 University of Virginia

Presented at the American Institute of Aeronautics and Astronautics SciTech
San Diego, California
January 7-11, 2019

NREL is a national laboratory of the U.S. Department of Energy
Office of Energy Efficiency & Renewable Energy
Operated by the Alliance for Sustainable Energy, LLC

Conference Paper
NREL/CP-5000-72658
March 2019

Contract No. DE-AC36-08GO28308

Design and Testing of a Scaled Demonstrator Turbine at the National Wind Technology Center

Preprint

Christopher J. Bay,[1] Rick Damiani,[1] Lee Jay Fingersh,[1] Scott Hughes,[1] Mayank Chetan,[2] Shulong Yao,[2] D. Todd Griffith,[2] Gavin K. Ananda,[3] Michael S. Selig,[3] Daniel S. Zalkind,[4] Lucy Y. Pao,[4] Dana Martin,[5] Kathryn E. Johnson,[5] Meghan Kaminski,[6] and Eric Loth[6]

1 National Renewable Energy Laboratory
2 University of Texas
3 University of Illinois
4 University of Colorado
5 Colorado School of Mines
6 University of Virginia

Suggested Citation
Bay, Christopher J., Rick Damiani, Lee Jay Fingersh, Scott Hughes, Mayank Chetan, Shulong Yao, D. Todd Griffith, Gavin K. Ananda, Michael S. Selig, Daniel S. Zalkind, Lucy Y. Pao, Dana Martin, Kathryn E. Johnson, Meghan Kaminski, and Eric Loth. *Design and Testing of a Scaled Demonstrator Turbine at the National Wind Technology Center: Preprint*. Golden, CO: National Renewable Energy Laboratory. NREL/CP-5000-72658. https://www.nrel.gov/docs/fy19osti/72658.pdf.

Contract No. DE-AC36-08GO28308

Conference Paper
NREL/CP-5000-72658
March 2019

National Renewable Energy Laboratory
15013 Denver West Parkway
Golden, CO 80401
303-275-3000 • www.nrel.gov

NOTICE

This work was authored by the National Renewable Energy Laboratory, operated by Alliance for Sustainable Energy, LLC, for the U.S. Department of Energy (DOE) under Contract No. DE-AC36-08GO28308. Funding provided by U.S. Department of Energy Office of Energy Efficiency and Renewable Energy Wind Energy Technologies Office. The views expressed herein do not necessarily represent the views of the DOE or the U.S. Government. The U.S. Government retains and the publisher, by accepting the article for publication, acknowledges that the U.S. Government retains a nonexclusive, paid-up, irrevocable, worldwide license to publish or reproduce the published form of this work, or allow others to do so, for U.S. Government purposes.

Cover Photos by Dennis Schroeder: (clockwise, left to right) NREL 51934, NREL 45897, NREL 42160, NREL 45891, NREL 48097, NREL 46526.

Design and Testing of a Scaled Demonstrator Turbine at the National Wind Technology Center

Christopher J. Bay*, Rick Damiani†, Lee Jay Fingersh‡, and Scott Hughes§
NREL, Golden, CO, 80401, USA

Mayank Chetan¶, Shulong Yao‖, and D. Todd Griffith**
University of Texas at Dallas, Richardson, TX, 75080

Gavin K. Ananda†† and Michael S. Selig‡‡
University of Illinois at Urbana-Champaign, Urbana, IL, 61801, USA

Daniel S. Zalkind§§ and Lucy Y. Pao¶¶
University of Colorado, Boulder, CO, 80309, USA

Dana Martin*** and Kathryn E. Johnson†††
Colorado School of Mines, Golden, CO, 80401, USA

Meghan Kaminski‡‡‡ and Eric Loth§§§
University of Virginia, Charlottesville, VA, USA

This paper discusses the design, manufacturing, and planned testing of a scaled demonstrator turbine as part of the Segmented Ultralight Morphing Rotor (SUMR) project funded by the Advanced Project Research Agency-Energy. The scaled demonstrator (SUMR-D) is a gravo-aeroelastically scaled version of a downwind, 13.2-MW SUMR design. This scaled rotor will be tested on the two-bladed Controls Advanced Research Turbine (CART2) at the National Wind Technology Center (NWTC) to verify the scaling methodology, and validate the aeroelastic modeling and control scheme. The design was done in an iterative fashion among six teams focused on aerodynamics, structures, and controls. This process included extensive load analysis, modification for manufacturability, adaptations required for testing on the CART2, and ground-based proof loading. The details of this process are presented here, concluding with planned testing and performance expectations.

I. Introduction

As the pursuit of renewable energy has intensified, wind energy has seen continued growth in installation and use. Over the last 5 years, the global installed capacity for wind turbines has nearly doubled to 539 GW [1]. As wind

*Engineer, NWTC, National Renewable Energy Laboratory (NREL), Golden, CO, 80401, USA
†Sr. Engineer, NWTC, National Renewable Energy Laboratory (NREL), Golden, CO, 80401, USA, AIAA Professional Member
‡Sr. Engineer, NWTC, NREL, Golden, CO, 80401, USA, AIAA Professional Member
§Sr. Engineer, NWTC, NREL, Golden, CO, 80401, USA
¶PhD Student, Department of Mechanical Engineering, University of Texas at Dallas, Richardson, TX, 75080
‖Ph.D. Student, Department of Mechanical Engineering, University of Texas at Dallas, Richardson, TX, 75080
**Associate Professor, Department of Mechanical Engineering, University of Texas at Dallas, Richardson, TX, 75080, AIAA Professional Member
††Ph.D. Student, Department of Aerospace Engineering, University of Illinois at Urbana-Champaign, Urbana, IL, 61801, USA, AIAA Student Member
‡‡Professor Emeritus and Research Professor, Department of Aerospace Engineering, University of Illinois at Urbana-Champaign, Urbana, IL, 61801, USA
§§Ph.D. Student, Department of Electrical Engineering, University of Colorado, Boulder, CO, 80309, USA
¶¶Palmer Endowed Chair Professor, Department of Electrical Engineering, University of Colorado, Boulder, CO, 80309, USA, AIAA Professional Member
***Ph.D. Student, Department of Electrical Engineering, Colorado School of Mines, Golden, CO, 80401, USA
†††Associate Professor, Department of Electrical Engineering, Colorado School of Mines, Golden, CO, 80401, USA
‡‡‡Ph.D. Student, Department of Mechanical and Aerospace Engineering, University of Virginia, Charlottesville, VA, 22903, USA
§§§Professor, Department of Mechanical and Aerospace Engineering, University of Virginia, Charlottesville, VA, 22903, USA

energy capacity has increased, so has wind turbine size. This increase in turbine size allows for more energy to be captured at a lower cost. However, as turbines continue to increase in size, so do the loads experienced within the system. In particular, the blades of traditional three-bladed, upwind turbines need to be sufficiently stiff to prevent the blades from striking the tower. As a result, if future developments follow existing trends in design and materials, more/stronger material will be required which translates into heavier mass/increased cost and increased loads on the entire system. Innovative designs and technologies will thus be required to address increasing aeroelastic loads. To address these issues, a two-bladed, downwind rotor concept known as the Segmented Ultralight Morphing Rotor (SUMR) has been proposed [2–4].

The SUMR concept utilizes a downwind rotor configuration and blade downwind coning to alleviate loads. The downwind layout partially relaxes the tower clearance design constraint, whereas the coning allows for the resultant blade loads to be better aligned with the blade axis. These factors, coupled with a dedicated control system, enable the deployment of a lighter and more flexible rotor. This, in turn, promises to further lower the cost of wind energy.

A team of six institutions: University of Virginia, University of Colorado Boulder, Colorado School of Mines, University of Texas at Dallas, University of Illinois at Urbana-Champaign, and the National Renewable Energy Laboratory (NREL) have been studying this concept with funding support from the Advanced Research Projects Agency-Energy. The team has been working toward developing a 50-MW SUMR rotor. In this process, an initial 13-MW SUMR rotor (SUMR-13) was designed and modeled in aeroelastic simulations to understand the issues with such extreme-scale turbines. To validate SUMR-13's numerical model, a field experiment was devised that would use a downscaled version of the SUMR-13 rotor on an existing turbine; we call this experiment the SUMR-Demonstrator (SUMR-D). The SUMR-D will be tested at the National Wind Technology Center (NWTC) at NREL, near Boulder, Colorado. Specifically, gravo-aeroelastically scaled blades were manufactured and installed on the two-bladed Controls Advanced Research Turbine (CART2).

This paper details the design and manufacturing process for the scaled demonstrator model. In Section II, a description of the CART2 and its relevant specifications will be given, focusing on its operating parameters and control philosophy. The CART2 description will be followed by an overview of the SUMR-D design steps in Section III. This overview will include adjustments that had to be made for the blade to be manufacturable, installable, and operable on the CART2. Sections IV and V introduce the reliability verification efforts, including the design load case (DLC) simulations, the simulation software used, and the analysis of the DLCs for design and safe operation. The manufacturing of the SUMR-D blades and required adapters is covered in Sections VI and VII. Sections VIII-X provide detail regarding the analysis of the pitch actuators, the ground-based proof loading, and the installation of the SUMR-D rotor. Finally, Sections XI and XII discuss goals for the field campaign and future work and conclusions.

II. CART2 Specifications

The upwind CART2 (see Figure 1) located at the NWTC is a specially instrumented turbine used to conduct state-of-the-art wind turbine control research. It is a modified Westinghouse WTG-600 wind turbine that was originally installed on the island of Oahu, Hawaii, and was operated commercially for about 10 years [5]. In 1996, it was shipped to the NWTC and instrumented with additional sensors and equipment to accommodate experiments to be performed in the research of advanced wind turbine control architectures. The pitch system was upgraded from being hydraulically actuated to an electro-mechanical system hosting a servo motor coupled to a gearing system to allow for high band-width individual pitch control. Additionally, the generator and power electronics were upgraded for a 650-kW squirrel-cage, induction-speed generator with a variable-speed mode [5]. The additional instrumentation included accelerometers in the nacelle recording tower-top dynamics, along with tower and blade strain gauges. The turbine hosts these additional sensors along with a PXI (PCI eXtensions for Instrumentation) in conjunction with real-time control and a 400-Hz LabVIEW data acquisition system to provide performance and safety control during operation, and serve as a platform for advanced control architecture testing and analysis.

The CART2 turbine configuration has a rotor diameter of 43.3 m and reaches a rated generator power of 600 kW near a wind speed of 11 m/s [6]. The maximum aerodynamic torque generated by the rotor is 162 kNm at a rated rotor angular velocity of 41.7 rpm, commanding 3.524 kNm of applied generator torque for rated operation. The turbine characteristics are presented in Table 1 along with some key frequencies of turbine components.

Fig. 1 A picture of the CART2 in an upwind configuration (courtesy of Lee Jay Fingersh).

Table 1 Summary of key turbine characteristics and component frequencies needed for controller development [5, 6].

Parameter	Value	Units	Parameter	Value	Units
Minimum Generator Speed	1295	rpm	Tilt angle of rotor to horizontal	3.77	deg
Rated Generator Speed	1800	rpm	Cone angle of rotor	0	deg
Rated Generator Electrical Power	600	kW	Rotor overhang	3.858	m
Rated Rotor Speed	41.7	rpm	Position of rotor relative to tower	Upwind	(-)
Maximum Rotor Speed	58	rpm	Cut in wind speed	4	m/s
Generator Torque Set Point	3524.36	N-m	Cut out wind speed	25	m/s
Maximum Rotor Torque	162000	N-m	First Rotor In-Plane Mode	4.31	Hz
Fine Pitch	-1	deg	Rated Rotational Frequency (1P)	0.695	Hz
Maximum Negative Pitch Rate	-18	deg/s	Blade Passing Frequency (2P)	1.39	Hz
Maximum Positive Pitch Rate	18	deg/s	First Fore-Aft Tower Mode	0.88	Hz
Rotor Diameter	43.3	m	First Rotor Out-of-Plane Mode	2.22	Hz
Number of Blades	2	(-)	Drivetrain Torsion	3.36	Hz
Tower Height	34.862	m			

In preparation for the SUMR-D testing campaign, the turbine was modified to operate in a downwind configuration with a highly coned rotor. The controller operating set points were customized to follow a gravo-aeroelastically scaled trajectory. Power derating followed from the applied scaling methodology that seeks to maintain nondimensionalized frequencies and deflections of the blades between SUMR-13 and SUMR-D, as detailed in [4].

III. Overview of Design Steps

There were several steps in the design, analysis, manufacturing, testing, and installation of the SUMR-D blades. This paper includes an overview of the steps that were taken, with further details provided in additional publications [2–4, 7–9]. First, the aerodynamic design will be introduced, followed by the structural design. Then, modifications to the CART2 for the SUMR-D field campaign and controller development will be discussed. Lastly, an overview of the reliability verification required to do this demonstration at the NWTC will be provided at the end of this section.

A. Aerodynamic Design

The rotor and the individual airfoil sections of the SUMR-13 were designed separately using an inverse design approach where the desired aerodynamic performance parameters were prescribed and the geometry that would yield that performance was obtained. The two design tools used for blade and airfoil design were PROPID [10, 11] and PROFOIL, [12, 13] respectively. PROPID is an inverse design tool used to design the wind turbine rotor geometry itself. In PROPID, the desired performance from the rotor is specified via prescription of the rated power, operating tip-speed ratio, average and rated wind speeds, axial induction distribution along the blade length, and the C_L distribution along the blade length, usually corresponding to the highest L/D ratio of each of the airfoil cross sections. Based on the aforementioned design parameters, the geometry of the rotor is obtained in terms of rotor diameter, blade pitch, and blade chord and twist distributions. PROFOIL, which is also an inverse design tool, is used for airfoil design. The desired airfoil performance is set by prescribing the appropriate velocity profiles over the airfoil and the tool returns the airfoil geometry that yields that profile. The airfoil geometry is then analyzed in XFOIL [14, 15] and based on the required performance, the prescribed velocity profiles are adjusted again. The process is iterated to finally converge to an optimum airfoil design. Figure 2 illustrates the inverse design methodology of PROFOIL and PROPID in a graphical manner.

As discussed in detail in Ref. [16], the actual SUMR-13 rotor design process involved initially setting a blade thickness distribution based on historical precedence and input from the structures team. The airfoils were designed using PROFOIL by maximizing L/D at specific operating design lift coefficients. Based on the expected size of the rotor radius to produce a rated power of 13.2 MW (R = 100 m), the operating tip-speed ratio (TSR = 9.5), and the average and rated wind speeds (V_{avg} = 8.5 m/s, V_{rated} = 11.3 m/s), a range of Reynolds numbers was estimated. The SUMR-13 wind turbine rotor blades were expected to operate within a range of Reynolds numbers varying from 4,000,000 toward the hub to as high as 15,000,000 near the tip. Therefore, to leverage the best aerodynamic performance from the airfoils at such high Reynolds numbers combined with various structural requirements, the F1-series of flatback airfoils were designed in PROFOIL. Following that, the blade pitch, radius, and chord and twist distribution were designed using PROPID. The blade design and airfoil performance data was then converted to a format to be used as an input to OpenFAST, NREL's aero-hydro-servo-elastic code [17]. With the aerodynamic design completed, a few iterations were carried out between the controls and structural design teams with a threefold objective. The first goal was to maximize power output at the average and rated wind speeds specified [18, 19]. The second objective was to ensure that predicted structural loads were within allowable limits following the International Electrotechnical Commision (IEC) [20] standards. The third objective was to minimize rotor mass, therefore demonstrating a reduction in rotor costs via the SUMR configuration. The final SUMR-13 design specifications are shown in Table 2.

The SUMR-D blade was then geometrically scaled from the SUMR-13 to a blade length of 20.87 m. No changes to the airfoil shape or planform were made, hence the aerodynamic efficiency of the SUMR-D blades is lower than the SUMR-13 blades because the airfoils will be operating at suboptimal Reynolds numbers. This was deemed acceptable as the focus of the SUMR-D test campaign is not on power production, and fine tuning of the pitch setting (see Section III.D) can restore most of the desired blade element force ratios.

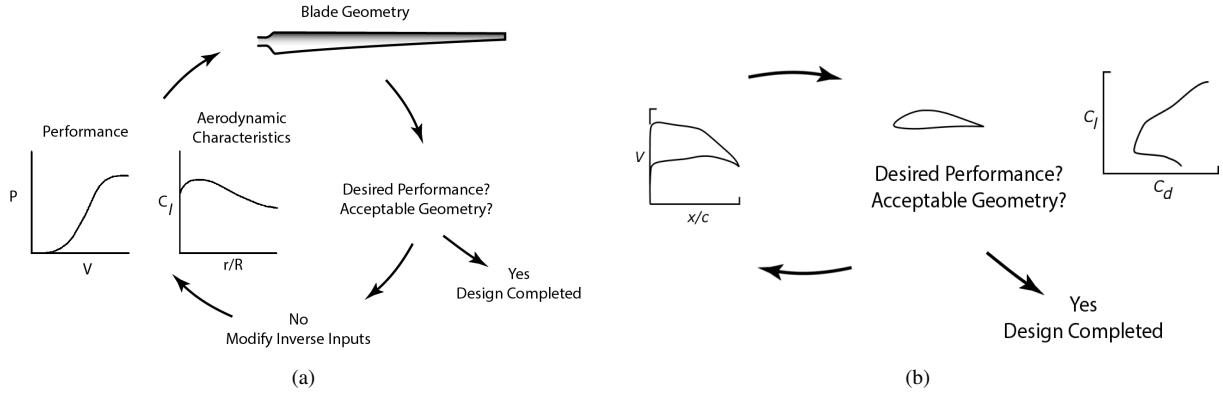

Fig. 2 Inverse design tools methodology description: (a) PROFOIL for airfoil design and (b) PROPID for rotor design.

Table 2 SUMR-13 and SUMR-D rotor parameters

Metric	SUMR-13	SUMR-D	CART2
Rated Power (P_{rated})	13.2 MW	53.9 kW	600 kW
Rated Wind Speed (V_{rated})	11.3 m/s	5.05 m/s	12.7 m/s
Cut-In Wind Speed (V_{cut-in})	5 m/s	3 m/s	4 m/s
Cut-Out Wind Speed ($V_{cut-out}$)	25 m/s	11 m/s	25 m/s
Rotor Radius (R)	106.85 m	22.25 m	21.65 m
Rated Rotor Speed (Ω)	9.54 RPM	21.47 RPM	41.7 RPM
Tip-Speed Ratio (TSR)	9.5	9.5	7.44
Cone Angle (β)	12.5 deg	12.5 deg	0 deg
Blade Mass (m_{blade})	55,700 kg	990 kg	2,126 kg
Rotor Mass (m_{rotor})	111,400 kg	8,988 kg	10,104 kg

B. Structural Design

The structural design for the SUMR-D had to satisfy both the novel scaling methodology and the traditional safety requirements for the highly turbulent NWTC test site. By changing the spar cap, shear webs, and core material quantities and dimensions, a good agreement was reached between the final blade structural properties and the target scaled values. The blade structure was also verified against loads calculated via OpenFAST simulations.

ANSYS APDL [21] was used for the structural (static/buckling) analysis of the blade. The loading conditions used in ANSYS were derived from extreme root bending moment cases that generated the load distributions shown in Figure 3, which will be further discussed in Section IV. For the static loading verification, it was ensured that the maximum von-Mises strain was below the allowable maximum strain of the materials and that the maximum deflection was less than the allowable value to avoid tower strike.

During the blade manufacturing phase, the structural model in ANSYS was updated to incorporate the mass increases caused by additional ply extensions and glue lips. More details about the design of the SUMR-D blade can be found in [8].

C. Modifications for Manufacturing/Use on CART2

As detailed in Section II, the CART2 was selected as the testing platform for the SUMR rotor concept. However, the basic turbine layout was extensively modified to enable the SUMR-D test to occur on the CART2. Some of the major considerations included configuring the CART2 to run in downwind mode. For example, the new rotor and blade orientation had to be reversed from the usual clockwise operation to maintain the original rotation direction of the drivetrain. The turbine yaw control system was reset to operate with a 180-deg offset, and the yaw limits adjusted accordingly. The pitch system had to be reversed in direction, with the pitch settings for "run" (0 degrees) and "feather" (90 degrees) swapped because the gearing is limited to an arc of approximately 100 deg. To create a downwind coning of the rotor while maintaining the existing pitch actuators, a special blade adapter to connect the blade to the hub was designed and manufactured. The adapter flange design had to account for the pitch actuation requirements and the asymmetric bolt pattern at the hub (see Section VII). The downwind operation also required the wind direction sensor on the nacelle to be rotated 180 degrees and recalibrated.

From an analysis conducted specifically to determine the optimal coning angle, it was determined that 12.5 degrees would give maximum performance while minimizing the root bending moment for the SUMR-13. This angle was maintained for the SUMR-D configuration. Finally, an eigenanalysis of the SUMR-D blade and CART2 system was performed to identify key operating conditions to control for and/or avoid.

D. Controller Development

The controller had the same structure that was used in the SUMR-13 design process, but retuned through an iterative process detailed in [19]. This required several iterations between the different groups within the team, requiring structural redesigns and aerodynamic reanalysis. In the end, several changes to the controller were needed. To compensate

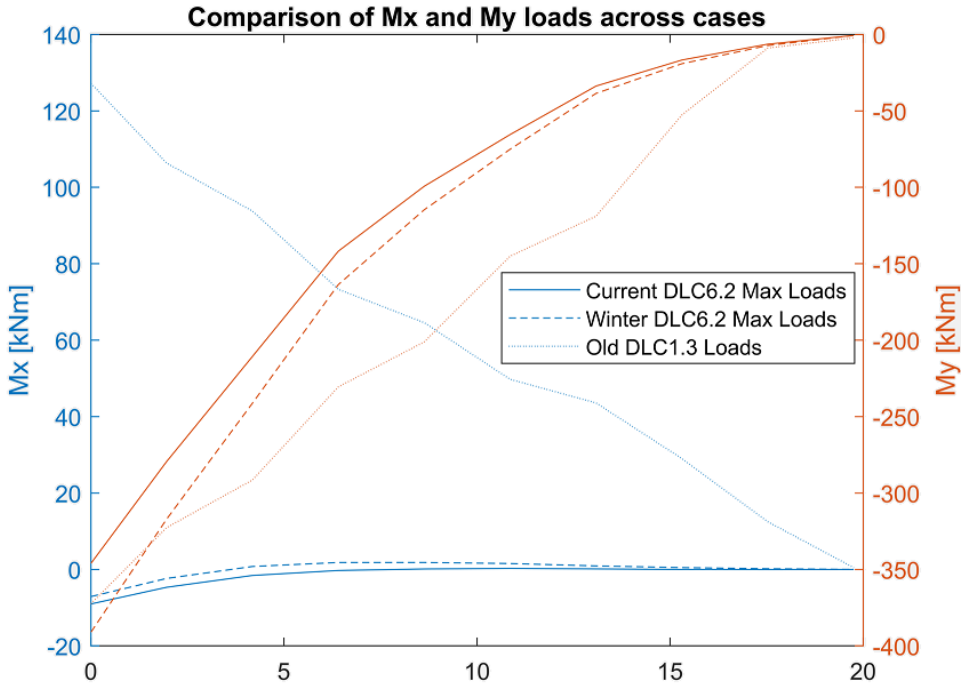

Fig. 3 Distribution of Mx (on the left y-axis, shown in blue) and My (on the right y-axis shown in orange) loads along the blade span.

for a less-than-ideal aerodynamic scaling, the run pitch of the SUMR-D blade was decreased by rotating the blade by -5 degrees relative to the run pitch on the adapter bolt pattern. This rotation allows the SUMR-D to better match the nondimensional deflection values predicted for the SUMR-13 and to better approximate the associated ratios of centrifugal force to thrust force along the blade span. The rotation magnitude was found through OpenFAST simulations optimizing the run-pitch angle to arrive at a better match of the SUMR-13 scaled values. More details can be found in [9]. At the same time, this fixed clocking does not reduce the limited range of pitch actuation and thus does not preclude further pitching toward feather if it is deemed necessary during testing. The supervisory controller for CART2 [22] remains in effect to protect the turbine, updated for downwind operation.

E. Reliability Verification

To ensure safe operation of the SUMR-D blades on the CART2, several DLCs were simulated and analyzed. These cases were required by the NWTC and used to identify the load distribution for the ground-based proof loading of the blades. Several operating points, potential control/actuator faults, normal and emergency shutdowns, as well as different parked conditions were included in the analysis, as shown in Table 3. The results and subsequent analysis of these DLCs are discussed in Section IV, along with information on the simulation setup, differences between ElastoDyn- and BeamDyn-based aero-servo-elastic simulations, and analysis to determine the possibility of testing during high-speed winter winds.

IV. DLCs and Analysis

The SUMR-D design was tested across several wind conditions and operating ranges according to Ref. [20]. The specific simulated conditions are shown in Table 3. Normal power production was simulated with different wind field regimes: normal turbulence model (NTM, DLC 1.1 [20]), extreme turbulence model (ETM, DLC 1.3 [20]), and extreme coherent gust with direction change (ECD, DLC 1.4 [20]).

Examined faults during power production included (a) losing the ability to control a single blade either stuck at its last commanded position or that pitches toward "run" (0 degrees) at the highest rate possible and (b) grid loss. For

Table 3 Summary of SUMR-D DLCs Analyzed

Turbine State	DLC	Wind Condition	Other Conditions
Power Production	1.1	Normal turbulence model with wind speeds from cut-in (2 m/s) to cut-out (11 m/s)	
	1.3	Extreme turbulence model (ETM) with wind speeds from cut-in (2 m/s) to cut-out (11 m/s)	
	1.4	Extreme coherent gust with direction change with wind speeds at rated (5 m/s) and +/- 1 m/s around rated	
Power Production with Fault	2.2	ETM with wind speeds from cut-in (2 m/s) to cut-out (11 m/s)	1) Loss of pitch authority on 1 blade (stuck) 2) Loss of pitch authority on 1 blade (runaway) 3) Electrical grid power loss
	2.3	Extreme operating gust with wind speeds at rated (5 m/s), +/- 1 m/s around rated, and cut-out (11 m/s)	1) Loss of pitch authority on 1 blade (stuck) 2) Loss of pitch authority on 1 blade (runaway) 3) Electrical grid power loss
Emergency Shutdown	5.1	ETM with wind speeds +/- 1 m/s around rated (5 m/s) and cut-out	1) Normal stop with blade pitch rate of 12 deg/s 2) Emergency stop with blade pitch rate of 18 deg/s and rotor brake applied
Parked with Rotor Idling	6.1	Extreme wind speed model with avg. wind speed of 28.57 m/s	Rotor idling with blades fully feathered (90 deg); simulate across 0-350-deg yaw misalignments in 10-deg increments
Parked with Rotor Locked	6.2	Extreme wind speed model with avg. wind speed of 28.57 m/s	Rotor locked with blades fully stalled (0 deg); simulate across 0-350-deg yaw misalignments in 10-deg increments

the CART2/SUMR-D, when the turbine experiences a grid loss, a back-up battery system is used to pitch the blades to "feather" (90 degrees) and the emergency brake is applied, causing a rapid slowdown and stop of the rotor. This rotor brake is normally held open when energized, so upon power loss, the brake is immediately applied. There is an additional rotor brake that is normally open and then closes when energized, which is used during other emergency shutdown routines. These faults were simulated with two types of wind fields: ETM (DLC 2.2 [20]) and extreme operating gust (EOG, DLC 2.3 [20]).

The emergency shutdown case (DLC 5.1 [20]) was simulated at and near rated as well as cut-out. Additionally, two types of emergency stops were simulated: a normal stop, which entails pitching the blades to feather at a rate of 12 deg/sec and allowing the rotor to idle, and an emergency stop, which pitches the blades to feather at a faster rate of 18 deg/sec and applies the rotor brake.

Finally, two parked DLCs (based on DLC 6.1 and 6.2 [20]) were simulated. In the first load case, the blades were feathered (90 degrees) with idling rotor (the brake is not applied). This was simulated with an extreme wind speed model (EWM) producing a maximum gust of 45 m/s. The second parked DLC was simulated with the same wind conditions as the first, but the turbine was parked with the blades pitched to "run" (0 degrees) and the rotor brake engaged. While unlikely, this case is meant to investigate some of the worst-case conditions the turbine could experience. Both cases accounted for yaw misalignments from 0 to 350 degrees in 10-deg increments to identify worst-case wind directions. The calculated probability of yearly exceedance of a 45-m/s wind speed is 0.54; accounting for the adopted safety factors

(minimum material partial safety factor of 2.04 and load factor equal to 1.35) brings the equivalent gust speed to ~75 m/s and the probability of its exceedance down to less than 0.1. The probability is even lower when accounting for the combined unlikely event of rotor locked and large yaw errors (> 20 degrees). DLC 6.2 produced the highest loads that were used to drive the structural design and proof-load test.

The aero-servo-elastic simulations were all carried out in OpenFAST for which a model of the SUMR-D/CART2 was produced. Controller development was done in Simulink [23]. The latest version of the aerodynamics module AeroDyn (AD v15) was used with OpenFAST. For the blade structural dynamics, the module ElastoDyn was used for all of the simulated DLCs. In addition to ElastoDyn, the advanced blade modeling module BeamDyn [17] was used to check a handful of high-load producing cases. ElastoDyn can capture the majority of the physics of the SUMR-D blade and it is less computationally expensive than BeamDyn. ElastoDyn, however, requires that the pitch axis and the blade axis be aligned, which is not the case for the SUMR-D blade-adapter configuration. Because of the precone adapter (see Section VII), the pitch axis and blade axis are offset by 12.5 degrees. This becomes more important for large pitch angle variations wherein the blade is swept along a conical surface about the pitch actuation axis as opposed to being rotated about the blade axis. BeamDyn can capture this effect, but requires much more computational resources. Therefore, ElastoDyn was first used across all the DLCs to identify the highest load cases, which were then rerun with BeamDyn to improve the load prediction accuracy.

Figure 4 shows the results of the OpenFAST simulations run for the DLCs described in Table 3. Specifically, the resultant root blade bending moments are shown, as this information was used to inform the structural design detailed in [8]. Each dot and plus sign within the DLCs represent an individual simulation. The boxes show the median (50%) and quartiles (25% and 75%) for the respective DLC. The whiskers show the cases below and above the 25% and 75% quartiles that are not considered outliers. The outliers are specifically represented by plus signs. It can be observed that the highest load (391 kNm) occurred in a DLC 6.2 simulation. This case, besides having the rotor locked with the blades pitched to "run" (0 degrees), simulated a 180-deg yaw misalignment, effectively having the SUMR-D pointed like an upwind turbine. DLC 2.2 shows an outlier close to the maximum DLC 6.2 value. This was from one of the cases run with BeamDyn. This analysis included additional winter wind cases for DLC 6.2 that were beyond those initially determined in the project. It was desired to keep the blades up over the winter to capture additional data, thus the additional winter wind cases were added to test for survivability. At the NWTC, this is important as the winter can see more extreme wind speeds than the other seasons. It was from these DLC 6.2 winter wind cases that the value used for the structural design and ultimately the proof load that was applied to the blade during ground proof-testing was determined. The proof testing is detailed in Section IX.

In addition to root blade bending moments, of particular interest were the blade tip deflections. With a lighter, more flexible blade structure, one of the main concerns was deflection of the blade such that the blade could strike the tower. Figure 5 shows the maximum out-of-plane deflections (OopDefl) for blades 1 and 2. Again, the DLC 6.2 case shows the maximum deflection of -3.7 m, which coincides with the same maximum root blade bending moment case. Fortunately, the admissible deflection is -4.02 m.

Figures 6 and 7 compare results for blade 1 root bending moments from a DLC 5.1 simulation run with ElastoDyn and BeamDyn, respectively. DLC 5.1 simulates an emergency stop, which in this case happened at 250 s near the cut-out wind speed of 11 m/s. The first 100 s of the simulation are used for startup transients to settle out and are not included in the analysis. The peak load occurs shortly after the emergency stop, with BeamDyn showing a higher load than ElastoDyn. The other DLCs that were checked with BeamDyn (DLC 1.3 and DLC 2.2) showed higher loads, but none of the loads exceeded the maximum load from DLC 6.2 simulated with ElastoDyn. DLC 6.2 was not simulated with BeamDyn as it is a nonoperational (parked) case and could be captured with ElastoDyn.

V. Load Rose Analysis of Maximum Blade Loadings

During the study, the largest root blade bending moments were calculated to be mostly edgewise (i.e., predominantly aligned along the y-axis [see also Figure 8]), a vector analysis of the maximum moments was performed to identify other off-axis (not predominantly along the x or y direction) loads that could cause buckling or other structural failures. Resultant loads were projected along angular sectors around the blade axis and visualized in a load rose format. This was done at six airfoil stations along the blade span. The entire DLC suite of simulations was sampled, and the data shown represent the maximum load (kNm) from all the DLCs in each angular sector. The black vector represents the maximum resultant moment from the DLCs described in Table 3. The dashed red and blue vectors represent the highest two loading cases from the additional test performed with the winter wind conditions described earlier. The times given in the legend indicate the time during the simulation that the maximum load occurred.

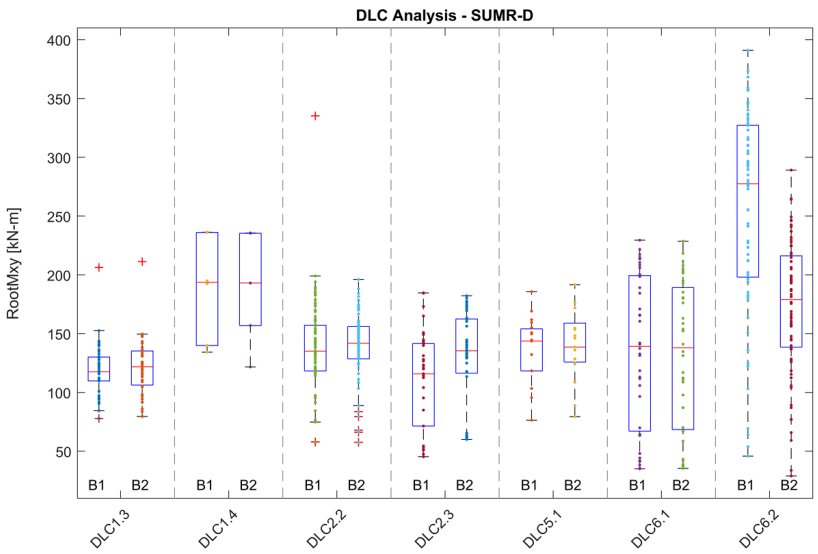

Fig. 4 Resultant root blade bending moments (RootMxy) across the DLCs that were analyzed.

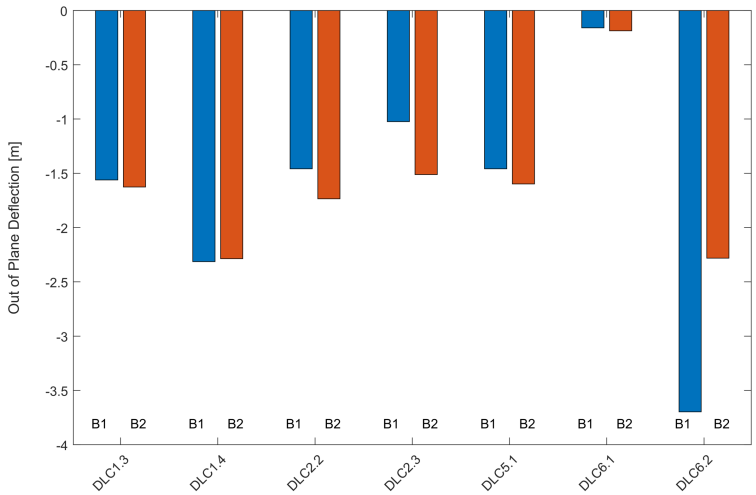

Fig. 5 Out-of-plane tip deflections (OoPDefl) across the DLCs that were analyzed.

Visualizing the data in such a manner made identifying other load cases to be checked by the structures team a straightforward process. Cases were selected from four sectors: sector 2 (27 degrees), sector 8 (135 degrees), and their complements (207 degrees and 315 degrees). The structural design was determined to be satisfactory for these loading specifications and the analysis is discussed in [8].

VI. Manufacturing of the Blades

The blades were manufactured by Janicki Industries (Janicki) in their facilities in the state of Washington under guidance from NREL. Given the available budget for this project, Janicki was directed to fabricate limited-production blade molds to reduce costs.

The tooling was manufactured starting from two plywood male templates (for the high-pressure side and suction side, respectively) that were covered by a wetlay of fiberglass sheets (facesheets) (see Figure 9). The facesheets were then first secured to fabricated steel frames and then covered with a special putty rendering a rough geometry of the molds. The putty was then machined by a high-precision, five-axis computer numerical control (CNC) mill that produced the

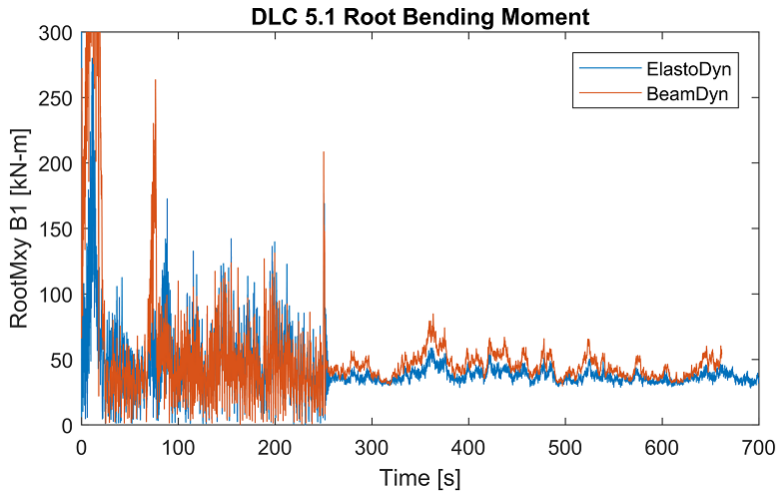

Fig. 6 Comparison of ElastoDyn and BeamDyn results.

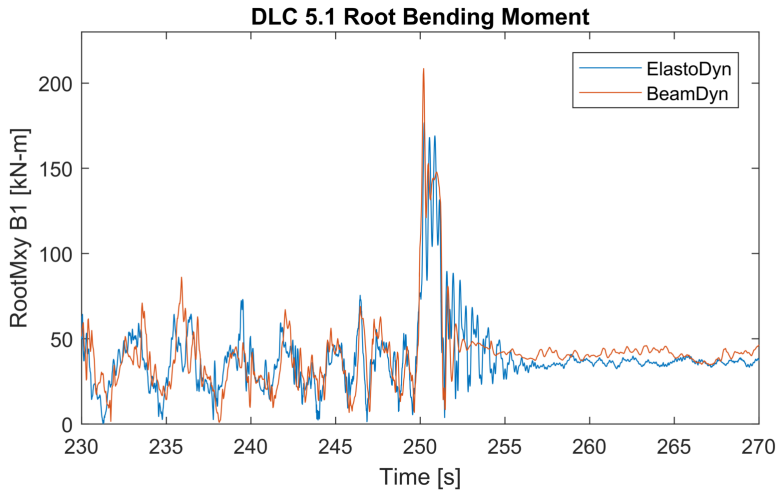

Fig. 7 A zoom-in of ElastoDyn and BeamDyn results from Figure 6.

final mold (see Figure 9(e)).

One of the biggest challenges in the blade manufacturing was overcoming the mold draft lock that was created by the large twist (some 34 degrees) of the blade airfoils. Special arrangements for glue lips and split lines had to be devised while clocking the outer mold line. Additionally, special fixtures had to be manufactured to position the rotated shear webs into the molds (see also Figure 10).

The blade material was manually cut and laid onto the two mold halves with the help of a laser guide. The spar cap and the root-build-up section were laid and infused in the mold together with the remainder of the fiber and core sheets. Vacuum-assisted resin transfer was used to infuse both halves of each blade. The shear webs were manufactured on flat tables, infused, and then bonded on the high-pressure side of the blade laminate. Balancing boxes were also installed on the same blade laminate. Before closing the tool, NREL staff installed strain gauges on both the upper and lower laminates near the second eigenmode antinode location (see Figure 11(a)). The strain gauges together form a full bridge for the flapwise and edgewise bending strain measurement. The final bonding, cure, and heated postcure were carried out after rotating and securing the suction-side laminate and mold onto the high-pressure mold. Once demolded, the blade leading-edge and trailing-edge bond lines were reinforced with overlaminates.

Special attention was given to the choice of the balsa core material used. This was done to minimize the resin uptake and therefore overall blade mass. The tip geometry was also revised to guarantee a smooth transition of the airfoil in an effort to reduce noise during turbine operation.

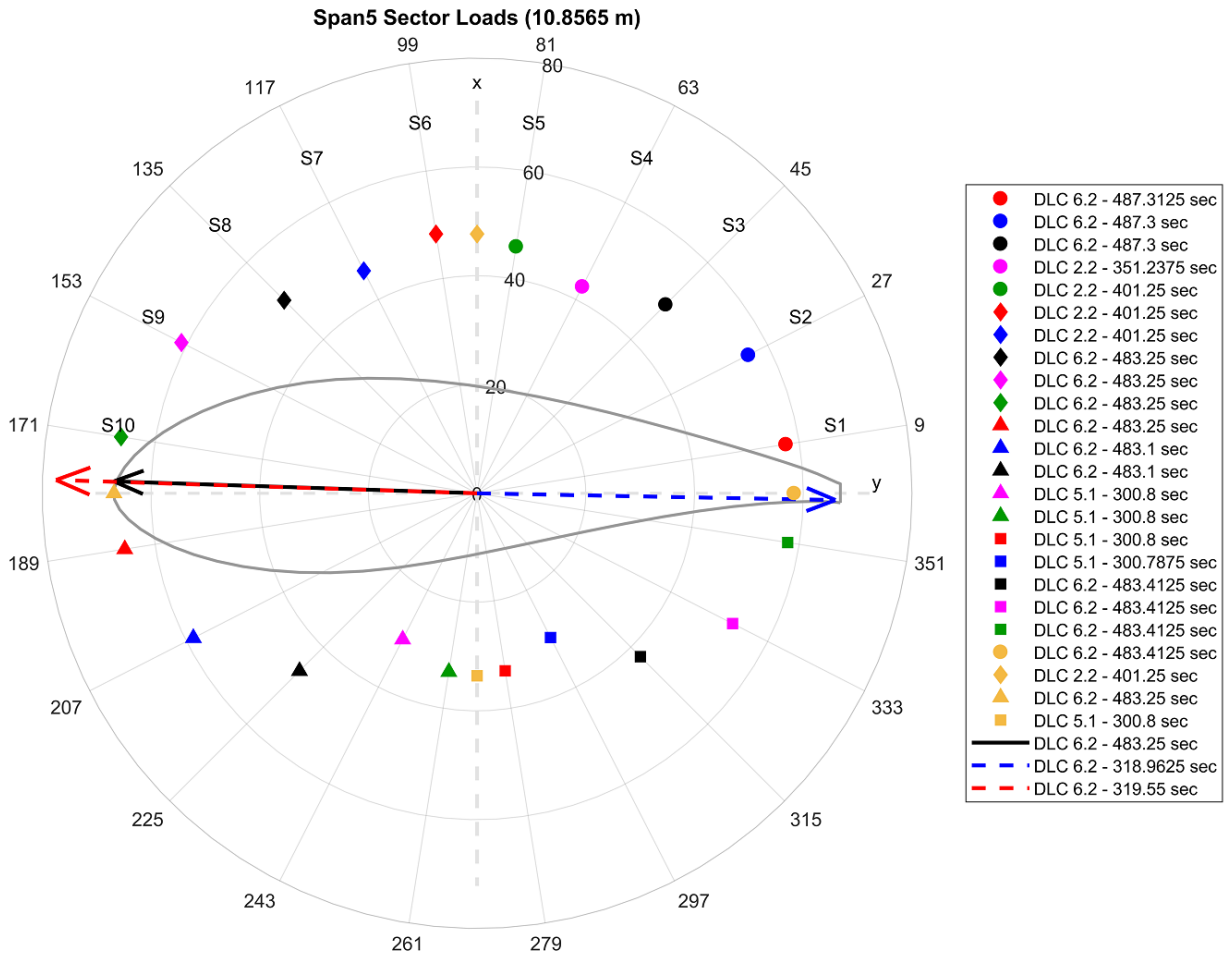

Fig. 8 Maximum bending moments across DLCs at 18-deg increments, x- and y-axes, and higher wind winter load cases. Each point represents the maximum load in that direction across all of the DLCs. The airfoil at the blade span location is outlined in grey for reference.

The SUMR-D inboard airfoils are of the flat-back type, whereas the outboard ones were designed with a sharp trailing edge in mind. However, partially because of the geometry scaling of the outer mold line, the airfoil trailing-edge thickness ended up being less than the cumulative thickness of the individual layers of materials in the trailing-edge-reinforcement region. The intersecting plies had to be truncated and postcure sanding was also performed to minimize this issue, but some aerodynamic imperfection can be expected. In addition to this aspect, the first manufactured blade suffered from upper mold slippage that caused a slight deformation of the leading edge. Nonetheless, it is expected that the blades will perform adequately for the field test, as discussed in Section XI.

NREL designed the hardware to connect the blade to the precone adapter (see Figure 12(a)). The hardware was comprised of threaded stud rods (24×M20 grade 10.9) and barrel nuts (60 mm diameter) on the blade side, and regular nuts on the adapter side. The bolted connection was verified for the highest loads calculated at the blade root from the aero-servo-elastic simulations. The verification included checks for bolt strength, joint opening, joint shear capacity, tear-out for the fiberglass, and thread stripping. Minimum margins of safety were calculated at 1.78 for the opening of the joint, and 1.59 for the bolt strength. Janicki machined the root to a flat surface, drilled holes for studs and barrel nuts with the same CNC mill used for the mold finishing, and shipped the blades to the NWTC (see Figure 12(b)).

(a) plywood template

(b) facesheet application

(c) facesheet connected to frame

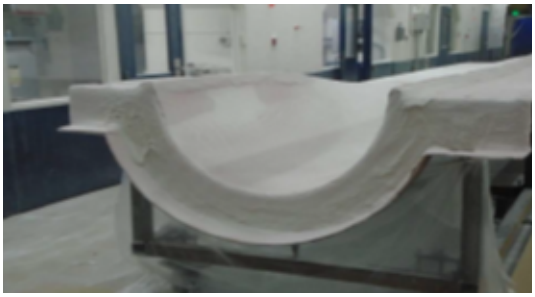

(d) putty application

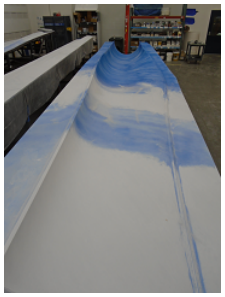

(e) final mold

Fig. 9 Fabrication of the blade molds.

(a) shear webs ready for final bonding

(b) blade tooling ready for bonding

Fig. 10 Views of the laminates and tooling prior to the final bonding phase.

VII. Blade Adapter

At the core of the SUMR concept is the blade load alignment, which is achieved through the rotor downwind preconing. Although future designs may include active coning (the ability to change the cone angle during operation), the SUMR-D demonstrator was designed with a fixed 12.5-deg coning angle because of budget constraints. Given that the CART2 hub has parallel spindle flanges (blade attachment flanges) and an oval bolt pattern (see Figure 13(a)), an adapter had to be designed and manufactured to both create the needed precone angle and allow for the connection to a circular blade root. The adapter also provides sufficient clearance between the blade and hub cover by extending the blade mounting flange further outboard. The designed adapter is shown in Figure 13(b). The two flanges of the

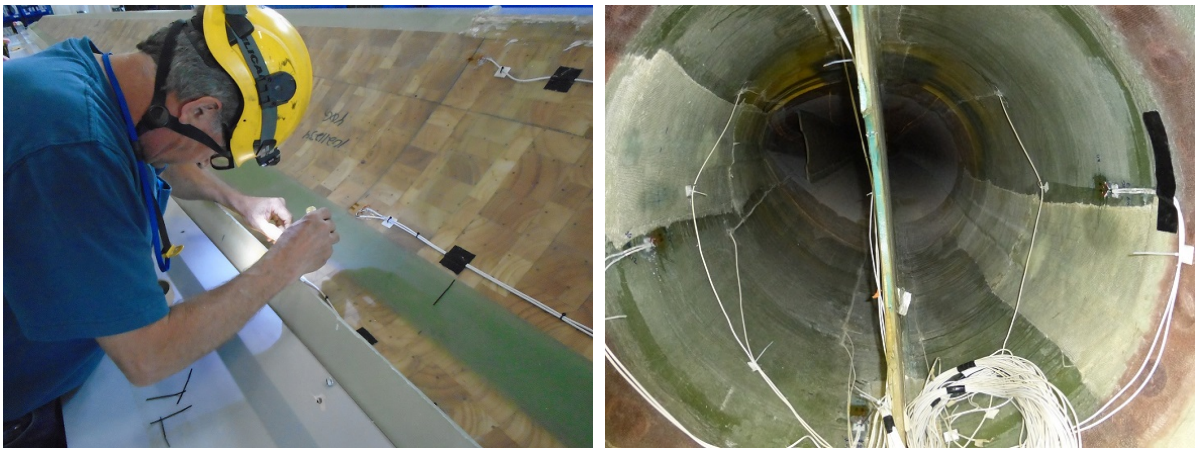

(a) strain gauge installation (b) view of strain gauges from the root

Fig. 11 Strain gauges were installed at approximately the midspan of the blade before the two blade halves were joined together. Additional root strain gauges were installed after bonding.

(a) blade root (b) blade transport

Fig. 12 (a) View of the SUMR-D blade root with hardware installed and (b) loading of blade 1 at Janicki Industries.

adapters are connected via a cylindrical sleeve and radial gussets. The two flanges form the 12.5-deg angle of precone and connect to the spindle plate and to the blade, respectively. The bolt pattern was clocked by -5 degrees to allow for the blade run pitch setting as mentioned in Section III.D. The design further included additional holes drilled into the edge of the mounting surfaces to serve as lift points for hoisting and rigging of the adapter as shown in Figure 18(a).

The adapter design was performed by NREL in collaboration with Janicki using the loads derived from the simulated DLCs as inputs with the load and material safety factors of 1.35 and 1.1, respectively. A finite-element analysis was performed to arrive at a final layout of the overall adapter as well as the weldments (see Figure 14(a)). A lot of care went into the manufacturing and welding of the adapter components, including appropriate dimension and shape tolerance prescriptions. Figure 14(b) shows initial tacking of the adapter subcomponents.

(a) View of the CART2 hub spindle.

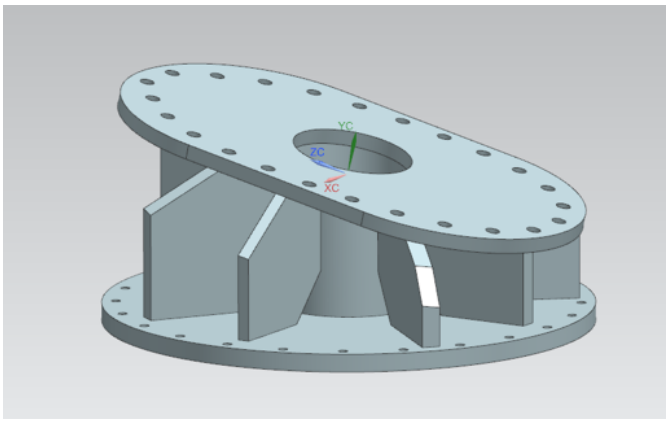

(b) CAD drawing of adapter.

Fig. 13 (a) The spindle plate with its atypical bolt pattern and (b) CAD drawing of the adapter required for mounting the SUMR-D blade to the CART2 hub while providing a 12.5-deg coning.

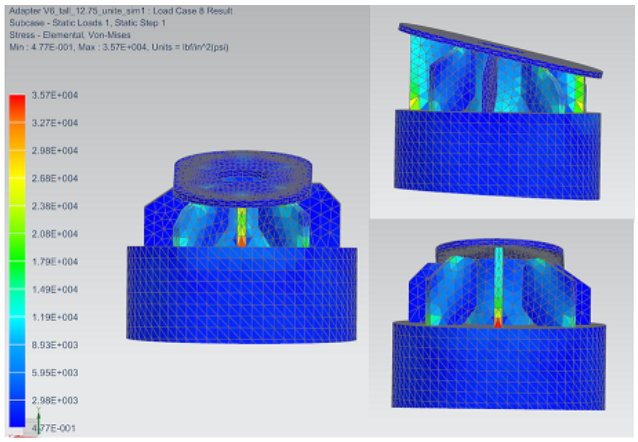

(a) Adapter FEA.

(b) Adapter being tacked for welding.

Fig. 14 (a) Finite-element analysis of the blade root adapter and (b) welding process to provide a 12.5-deg coning.

VIII. Torque Analysis of Pitch Actuators

Given the CART2 pitch actuation gearing and kinematics, pitching of the blades in the downwind configuration, required swapping of the normal run and feathered set points both in the controller and drive electronics, as well as mechanically. As shown in Figure 13(a), the spindle is asymmetrically placed about the pitch bearing axis. Normally, in the upwind configuration, the feathered spindle position is as shown in the figure. A 90-deg rotation of the spindle (counterclockwise in Figure 13(a)) would put the blade in the run position. The original CART2 blade has its quarter-chord axis aligned with the pitch axis. In the SUMR-D version of the CART2, however, that is not the case. First, the spindle position in Figure 13(a) is the actual run position for SUMR-D. Second, because of the coning, the blade center of mass is located forward of the pitch bearing, and so is the lift center. This creates an additional pitching moment that must be resisted by the pitch actuation system. It is therefore critical to verify that the existing CART2 pitch hardware architecture is capable of withstanding the extra loading.

Accounting for the resulting geometry and for loads calculated in the aero-servo-elastic simulations discussed earlier in this paper, contributions to the pitch actuation torque from blade root shear, axial force, edgewise bending moment, and torque about the blade axis were determined and appropriately combined. It was verified that under normal operation the pitch drive is able to sustain the applied torque. Under extreme events, there could be a temporary

slippage of the pitch set value, but that would not damage the components and would be restored in a few seconds.

IX. Ground Proof-Loading

Besides other safety requirements, a retrofit blade needs to undergo a proof-loading test to demonstrate adequate safety margins (besides other safety requirements). One of the SUMR-D blades (the first manufactured blade) was tested in the Structural Testing Laboratory at the NWTC. The test involved connecting the blade and its adapter to the 5.4-MNm test stand via a custom adapter plate that had to be designed and manufactured to match the SUMR-D adapter bolt hole pattern (see Figure 15(b)). The loads applied by winches at three saddle points were derived from the results of the OpenFAST simulations described in Section III.E. First, the two most critical distributions of flapwise bending moments (in the positive and negative direction, respectively) were selected. These distributions represented factored loads (1.35×) of the minimum and maximum root bending moments (-368 kNm and 391 kNm). Then, the positions of the saddles and applied load magnitudes were optimized to match the target load distributions (see Figure 15(c)). Edgewise static tests were not deemed necessary.

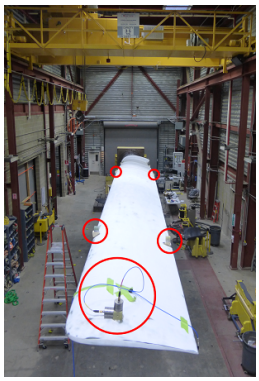

(a) Accelerometer installation.

(b) View of the blade and adapter on the test stand.

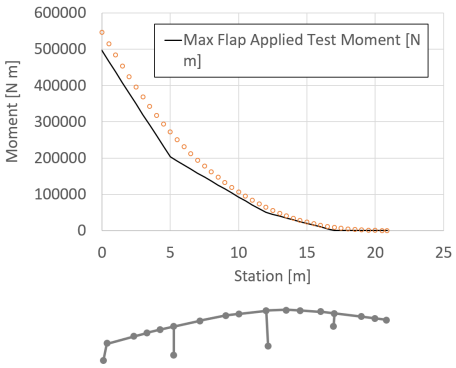

(c) Applied bending moment distribution.

Fig. 15 (a) Installation of the accelerometers on the SUMR-D blade to perform modal testing. (b) The SUMR-D blade and adapter mounted on the test stand. The 12.5 degrees of preconing are shown. (c) Target flapwise bending moment distribution along the blade span (circles) and achieved distribution with three saddle point loads.

The blade was rotated 180 degrees in between tests to execute the minimum and maximum pulls. A photo of the blade during one of the pulls is shown in Figure 16(a).

A third static pull was conducted to verify the blade structural integrity during blade installation. Specifically, with the blades attached to the CART2 hub, the rotor assembly would be lifted by two straps (one around the base of each blade) (see also Section X). Thus, this test was conducted to ensure that the blades could withstand the factored weight of the rotor assembly during installation.

The blade passed all the tests with minimal cosmetic damage on the suction surface. Localized delaminations occurred around pre-existing defects that were introduced during manufacturing. These voids were repaired solely for aerodynamic purposes (see Figure 16(b)).

An additional modal test was conducted to assess the eigenfrequencies, eigenmodes, and structural properties of the as-built blade. Accelerometers were installed at 24 different locations (see Figure 15(a) for examples of some installed locations). The test informed subsequent finite-element model updates that are discussed in [8].

X. Installation Aspects

Because the CART2 does not have a rotor lock and the torque caused by the weight of just one blade would overcome the capabilities of the rotor brake, the hub and rotor assembly had to be lowered to the ground to install the new SUMR-D blades. A cradle/stand was manufactured to hold the hub on the ground and allow for the blade swap. A picture of the SUMR-D rotor assembly on the stand is shown in Figure 17(a). The preconing of the SUMR-D blades from the adapter was an additional complication to the normal order of installation steps. As shown in Figure 17(a), the hub had to be

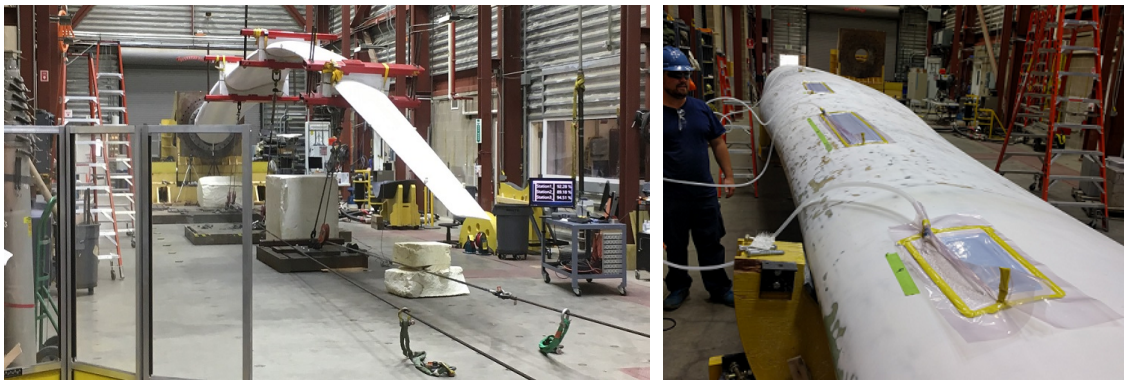

(a) Static test. (b) Delamination repairs.

Fig. 16 (a) The SUMR-D blade under maximum proof load. (b) Surface delamination occurred at a few locations and had to be repaired.

rotated by an angle equal to the precone angle (12.5 deg) for the blades to be installed; however, for the lift to occur safely, the blade roots needed to be in the same horizontal plane so that two straps of the same length could be used to lift the rotor and the rotor would not try to rotate about the hub during the lift.

Figure 17(b) shows the rotor assembly with the blades in the "feathered" position (90-deg pitch). This is how the blades were installed on the ground. For the lift, the blades were pitched to "run" (0-deg pitch), as shown in Figure 17(c), via a simple pitch controller that was developed to be used with the hub on the ground.

(a) Rotor-hub assembly on cradle.

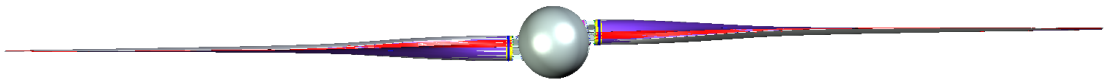

(b) Rendered view from downwind of the feathered rotor.

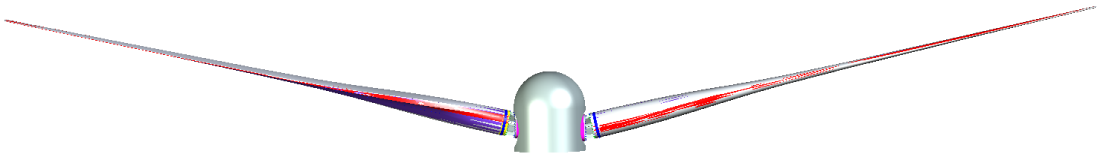

(c) Rendered view from above the operational rotor.

Fig. 17 (a) The hub was held by a special cradle (designed and manufactured by NREL), whereas the old blades were removed and the new blades were installed. (b) A rendering looking from downwind of the rotor assembly with the blades in a "feathered" position (90-deg pitch). (c) A rendering looking from above the rotor assembly with the blades in a "run" position (0-deg pitch).

After securing the rotor-hub assembly to the cradle and removing the original blades, it was discovered that a bearing protective ring was precluding the flush installation of the adapters to the spindle plates. The ring had to be turned

down to allow for the SUMR-D blade adapter installation. The pitch actuators were then pitched to the "feathered" position, and the hub was rotated about its central axis by 12.5 degrees. This rotation made the outer flange of each of the adapters vertical. Next, the blades were lifted and installed onto the adapters, following specified torquing sequences. With the blades installed, the pitch actuators were pitched back to the "run" configuration and the hub rotated by -12.5 degrees such that the blades were in the same horizontal plane. The new rotor assembly was lifted and fastened back to the CART2 nacelle, as shown in Figures 18(b)-(c). The electrical connections were later re-established to complete the SUMR-D installation.

(a) NWTC technicians install one of the blade adapters to the CART2 hub.

(b) A crane was used to lift the rotor to be installed on the nacelle.

(c) Technicians used bolts to realign the rotor with the nacelle and draw it in so it was fully secured.

Fig. 18 Photos taken during the installation process.

XI. Goals of Testing

There are several goals behind the SUMR-D test campaign. As previously mentioned, the SUMR-D is a gravo-aeroelastically downscaled version of a 13-MW turbine design, the SUMR-13. As such, the main goal is to capture the dynamic response of the full-scale turbine through a subscale demonstrator. This implies demonstrating that lighter-than-conventional blades can be used in a downwind, highly preconed configuration without compromising the safety and structural integrity of the system. To this end, besides operational cases, tests will be also performed under extreme wind events and parked conditions with yaw error, including normal and emergency shutdowns. Additionally, the two-bladed configuration will be operated with independent pitch control and locked teeter, to demonstrate advanced control architectures and techniques to abate the blade and tower response to the 1P and 2P forcing.

Ultimately, the test data will be used to validate OpenFAST and assess the validity of the scaling methods used. To this end, the tip deflection and blade loads will be measured and compared to OpenFAST predictions from simulations run with a fine-tuned aerodynamic and structural model. A successful validation will confirm the load reduction resulting from the load-alignment design, which is at the core of the SUMR concept.

If time and budget permit, we may investigate the wake of the downwind configuration and extract remote sensing (e.g., lidar) data, acoustic noise, as well as load and performance signals during normal and yaw-offset operations. Downwind turbines are also the subject of the International Energy Agency Research Task 40 [24], and these results will help inform that task on the structural dynamic response, fatigue loading performance, acoustics, and wake control efficacy of two-bladed downwind turbines.

Finally, future designs of the 25-MW and 50-MW turbines, SUMR-25 and SUMR-50, will benefit from the results of the experimental campaign and the associated verified scaling procedure together with all the lessons learned in the process.

XII. Future Work and Conclusions

This paper presents the process of designing and manufacturing two wind turbine blades for the purpose of a field demonstration test (SUMR-D) at the NWTC. Starting from a 13-MW design, a scaled version of the blades was generated, iteratively designed and analyzed, and manufactured. The blades were structurally tested with proof loads and installed onto a turbine at the NWTC. Thus far, the entire process has taken approximately 1.5 years and is continuing with the field test.

One conclusion from this process is that retrofitting an existing turbine for an unconventional configuration is laden with challenges, many of which are different from typycal rotor upgrades and difficult to predict at the beginning of the

project. Therefore, a critical analysis of the budget and schedule should be given significant attention to mitigate some of the unexpected obstacles, starting with the lessons learned from the SUMR-D endeavor.

Another conclusion is that to effectively optimize a wind turbine design from loading, to power production, to economic cost, an iterative design with an interdisciplinary team is needed. Breaking away from the traditional "linear" design process in which each team performs their task and gives the design to the next team, the authors were able to simultaneously generate a highly optimized blade design that pushes the limits of traditional blade mass and flexibility.

Ongoing work is focused on the field campaign of the SUMR-D and collecting and analyzing relevant data. The insights from this field campaign will allow for updating the scaling laws used to scale the SUMR-13 design to the SUMR-D and also informing the design of the SUMR-50 turbine.

Acknowledgments

This work has been supported by the Advanced Research Projects Agency-Energy under award number DE-AR0000667. Any opinions, findings, and conclusions or recommendations expressed in this material are those of the authors and do not necessarily reflect the views of the funding agencies. The authors would like to acknowledge the engineers, technicians, and support staff at the National Wind Technology Center, with whom this project and these efforts would not have been possible. Specifically, the authors would like to thank Tiffany Byrne, Scott Hughes, Bill Gage, Matthew O'Connell, Benjamin Anderson, Ryan Beach, Jason Roadman, Andy Scholbrock, Scott Wilde, Robert Goldhor, Simon Thao, and Garth Johnson for all their efforts and support, which are greatly appreciated. Further, the authors would like to acknowledge Janicki Industries for their contributions to the project.

This work was authored [in part] by the National Renewable Energy Laboratory, operated by the Alliance for Sustainable Energy, LLC, for the U.S. Department of Energy (DOE) under Contract No. DE-AC36-08GO28308. Funding provided by the U.S. Department of Energy Office of Energy Efficiency and Renewable Energy Wind Energy Technologies Office. The views expressed in the article do not necessarily represent the views of the DOE or the U.S. Government. The U.S. Government retains, and the publisher, by accepting the article for publication, acknowledges that the U.S. Government retains a nonexclusive, paid-up, irrevocable, worldwide license to publish or reproduce the published form of this work, or allow others to do so, for U.S. Government purposes.

References

[1] Global Wind Energy Council, "Global Wind Report - Annual Market Update," Tech. rep., GWEC, 2017. URL http://gwec.net/publications/global-wind-report-2/, bibtex: global_wind_energy_council_global_2017.

[2] Ichter, B., Steele, A., Loth, E., Moriarty, P., and Selig, M., "A morphing downwind-aligned rotor concept based on a 13-MW wind turbine," *Wind Energy*, Vol. 19, No. 4, 2015, pp. 625–637. doi:10.1002/we.1855, URL https://onlinelibrary.wiley.com/doi/abs/10.1002/we.1855.

[3] Loth, E., Steele, A., Qin, C., Ichter, B., Selig, M. S., and Moriarty, P., "Downwind pre-aligned rotors for extreme-scale wind turbines," *Wind Energy*, Vol. 20, No. 7, 2017, pp. 1241–1259. doi:10.1002/we.2092, URL https://onlinelibrary.wiley.com/doi/abs/10.1002/we.2092.

[4] Loth, E., Fingersh, L., Griffith, D., Kaminski, M., and Qin, C., "Gravo-Aeroelastically Scaling for Extreme-Scale Wind Turbines," *35th AIAA Applied Aerodynamics Conference*, AIAA AVIATION Forum, American Institute of Aeronautics and Astronautics, 2017, pp. 1–11. doi:10.2514/6.2017-4215, URL https://arc.aiaa.org/doi/10.2514/6.2017-4215.

[5] Fingersh, Lee Jay, and Johnson, Kathryn E, "Controls advanced research turbine (CART) commissioning and baseline data collection," Technical Report, National Renewable Energy Laboratory, Golden, CO, 2002.

[6] Bossanyi, E., Wright, A., and Fleming, P., "Controller field tests on the NREL CART2 turbine," *NREL*, 2010. doi:10.2172/1001440.

[7] Kaminski, M., Loth, E., Qin, C., and Griffith, D. T., "Gravo-Aeroelastic Scaling a 13.2 MW Wind Turbine Blade to a 1-meter Model," *Wind Energy Symposium*, AIAA SciTech Forum, American Institute of Aeronautics and Astronautics, 2018, pp. 1–11. doi:10.2514/6.2018-1731, URL https://arc.aiaa.org/doi/10.2514/6.2018-1731.

[8] Shulong Yao, D. Todd Griffith, Mayank Chetan, Christopher J. Bay, Rick Damiani, Meghan Kaminski, and Eric Loth, "Structural Design of a 1/5th Scale Gravo-Aeroelastic Scaled Wind Turbine Demonstrator Blade for Field Testing," *To be published*, American Institute of Aeronautics and Astronautics, San Diego, CA, 2019, pp. 1–11.

[9] Kaminski, M., Loth, E., Yao, S., Chetan, M., Griffith, D. T., Damiani, R., Martin, D., Bay, C. J., Johnson, K. E., Pao, L. Y., Qin, C., Ananda, G. K., and Selig, M., "Design and Ground Test for an Aeroelastically Scaled 13-MW Downwind Turbine at 20% Scale," *Wind Energy Science (pre-print)*, 2019.

[10] Selig, M. S., and Tangler, J. L., "Development of a multipoint inverse design method for horizontal axis wind turbines," *Wind Engineering*, Vol. 19, 1995, pp. 91–105.

[11] Michael S. Selig, "PROPID – Software for Horizontal-Axis Wind Turbine Design and Analysis," online, 1995. URL http://www.ae.illinois.edu/m-selig/propid.html.

[12] Selig, M. S., and Maughmer, M. D., "Generalized multipoint inverse airfoil design," *AIAA Journal*, Vol. 30, No. 11, 1992, pp. 2618–2625. doi:10.2514/3.11276, URL https://arc.aiaa.org/doi/abs/10.2514/3.11276.

[13] Selig, M. S., "Multi-point inverse design of isolated airfoils and airfoils in cascade in incompressible flow." PhD Dissertation, Dept. of Aerospace Engineering, Pennsylvania State Univ., University Park, PA, 1992.

[14] Drela, M., and Giles, M. B., "Viscous-inviscid analysis of transonic and low Reynolds number airfoils," *AIAA Journal*, Vol. 25, No. 10, 1987, pp. 1347–1355. doi:10.2514/3.9789, URL https://arc.aiaa.org/doi/10.2514/3.9789.

[15] Drela, M., "XFOIL: An Analysis and Design System for Low Reynolds Number Airfoils," *Low Reynolds Number Aerodynamics*, Lecture Notes in Engineering, Springer, Berlin, Heidelberg, 1989, pp. 1–12. doi:10.1007/978-3-642-84010-4_1, URL https://link.springer.com/chapter/10.1007/978-3-642-84010-4_1.

[16] Ananda, G. K., Bansal, S., and Selig, M. S., "Aerodynamic Design of the 13.2 MW SUMR-13i Wind Turbine Rotor," *2018 Wind Energy Symposium*, American Institute of Aeronautics and Astronautics, 2018, pp. 1–18. doi:10.2514/6.2018-0994, URL https://arc.aiaa.org/doi/abs/10.2514/6.2018-0994.

[17] National Renewable Energy Laboratory, "OpenFAST," online, 2018. URL https://nwtc.nrel.gov/OpenFAST.

[18] Martin, D. P., Johnson, K. E., Zalkind, D. S., and Pao, L. Y., "LPV-based torque control for an extreme-scale morphing wind turbine rotor," *American Control Conference*, 2017, pp. 1383–1388. doi:10.23919/ACC.2017.7963146.

[19] Zalkind, D. S., Pao, L. Y., Martin, D. P., and Johnson, K. E., "Models used for the simulation and control of a segmented ultralight morphing rotor," *IFAC-PapersOnLine*, Vol. 50, No. 1, 2017, pp. 4478–4483. doi:10.1016/j.ifacol.2017.08.377, URL http://www.sciencedirect.com/science/article/pii/S2405896317307218.

[20] International Electrotechnical Commission, "IEC 61400-1, Third Ed. 2005-2008. Wind Turbines – Part I: Design Requirements," Standard, IEC, 2005.

[21] ANSYS, Inc., "ANSYS," online, 2018. URL https://www.ansys.com.

[22] Johnson, K. E., and Fleming, P. A., "Development, implementation, and testing of fault detection strategies on the National Wind Technology Center's controls advanced research turbines," *Mechatronics*, Vol. 21, No. 4, 2011, pp. 728–736.

[23] MathWorks, "MATLAB," online, 2018. URL https://www.mathworks.com/products/matlab.html.

[24] IEA Wind, "Task 40," online, 2018. URL https://community.ieawind.org/task40/home.